nature COMMUNICATIONS

ARTICLE

Received 4 Jun 2015 | Accepted 17 Sep 2015 | Published 20 Oct 2015 | Updated 17 Nov 2015

DOI: 10.1038/ncomms9667 OPEN

Structural isomerism in gold nanoparticles revealed by X-ray crystallography

Shubo Tian[1], Yi-Zhi Li[2], Man-Bo Li[1], Jinyun Yuan[3], Jinlong Yang[3], Zhikun Wu[1] & Rongchao Jin[4]

Revealing structural isomerism in nanoparticles using single-crystal X-ray crystallography remains a largely unresolved task, although it has been theoretically predicted with some experimental clues. Here we report a pair of structural isomers, Au_{38T} and Au_{38Q}, as evidenced using electrospray ionization mass spectrometry, X-ray photoelectron spectroscopy, thermogravimetric analysis and indisputable single-crystal X-ray crystallography. The two isomers show different optical and catalytic properties, and differences in stability. In addition, the less stable Au_{38T} can be irreversibly transformed to the more stable Au_{38Q} at 50 °C in toluene. This work may represent an important advance in revealing structural isomerism at the nanoscale.

[1] Key Laboratory of Materials Physics, Anhui Key Laboratory of Nanomaterials and Nanotechnology, Institute of Solid State Physics, Chinese Academy of Sciences, Hefei, Anhui 230031, China. [2] State Key Laboratory of Coordination Chemistry, School of Chemistry and Chemical Engineering, Nanjing University, Nanjing 210093, China. [3] Hefei National Laboratory for Physical Sciences at the Microscale and Synergetic Innovation Center of Quantum Information and Quantum Physics, University of Science and Technology of China, Hefei, Anhui 230026, China. [4] Department of Chemistry, Carnegie Mellon University, Pittsburgh, Pennsylvania 15213, United States. Correspondence and requests for materials should be addressed to Z.W. (email: zkwu@issp.ac.cn) or to R.J. (email: rongchao@andrew.cmu.edu).

Structural isomerism in organic molecules is a common occurrence due to the bonding diversity of carbon. However, for nanoscale or even larger scale materials, experimental observation of structural isomerism has been largely impeded by the challenge of unravelling the intrinsic structure at the atomic level[1]. Nevertheless, theoretical and experimental efforts[2–8] in searching for structural isomerism in such materials continue, because such a finding would provide precise and insightful structure–property correlations and meaningful guidance for designing and synthesizing unique functional materials. The recently developed ultrasmall, thiolated metal nanoparticles (also called nanoclusters) provide opportunities for investigating structural isomerism, as they can now be controlled with atomic precision[9–20] and their structures can be resolved by single-crystal X-ray crystallography (SCXC) as well. To date, the structures of a series of thiolated metal nanoparticles with various sizes have been elucidated experimentally and theoretically[21–28]; however, to the best of our knowledge, no structural isomerism in thiolated metal nanoparticles has been reported, albeit $Au_{24}(SCH_2Ph\text{-}^tBu)_{20}$ and $Au_{24}(SePh)_{20}$ were revealed to have different Au_{24} core structures[29,30]. In a strict sense, $Au_{24}(SCH_2Ph\text{-}^tBu)_{20}$ and $Au_{24}(SePh)_{20}$ are not structural isomers, since their ligands are different. Thus, structural isomerism in thiolated nanoparticles remains a mystery.

In the current work, using a modified synthesis method for Au_{25}, we synthesize a nanocluster, whose composition is determined to be the same as that of the previously reported $Au_{38}(PET)_{24}$ (refs 31–33) (PET, phenylethanethiolate), as evidenced by electrospray ionization mass spectrometry (ESI–MS) in combination with X-ray photoelectron spectroscopy (XPS) and thermogravimetric analysis (TGA). SCXC reveals that the structure of this nanocluster is different from that of the previously reported structure[24]. To differentiate the two structures, the previous Au_{38} is denoted as Au_{38Q} and our nanocluster is denoted as Au_{38T} (where Q and T are the surname initial of the first author of the previous and current work, respectively). Au_{38T} and Au_{38Q} are therefore structural isomers and they represent the first pair of structural isomers in nanoparticles as revealed by SCXC, to the best of our knowledge. The two isomers exhibit distinctly different optical, stability and catalytic properties, and the less stable Au_{38T} can be irreversibly transformed to the more stable Au_{38Q} at 50 °C.

Results

Characterization. Au_{38T} was synthesized using a modified one-pot method[34] and isolated using preparative thin-layer chromatography (PTLC)[35,36]. ESI–MS was employed to determine the exact molecular mass and formula of the novel nanoparticle (note: caesium acetate was added to form positively charged adducts). Three distinct peaks centred at *m/z* 10910.186, 7317.312 and 5522.217 were observed in the mass spectrum (Fig. 1a). The peaks at *m/z* 10910.186 and 5522.217 (almost half of 10910.186) can be readily assigned to $[Au_{38}(PET)_{24}Cs]^+$ (theoretical *m/z* value: 10910.658; deviation: 0.472) and $[Au_{38}(PET)_{24}Cs_2]^{2+}$ (theoretical *m/z* value: 5522.772; deviation: 0.555), respectively. The peak at m/z 7317.312 can be assigned to $Au_{26}(PET)_{16}$ (theoretical *m/z* value: 7316.818; deviation: 0.494), which could be a fragment of $Au_{38}(PET)_{24}$, because the nanoparticles are monodisperse, as demonstrated by TLC, and it is also observed in the ESI spectrum of Au_{38Q} (see below). Based on the ESI–MS results, it is concluded that the as-prepared nanoparticle is neutral, and that its composition is $Au_{38}(PET)_{24}$, which is also corroborated by the TGA and XPS. TGA shows a weight loss of 30.39 wt% (Fig. 1b), corresponding to the theoretical loss of 30.55 wt% according to the formula. No other elements (including Cl, Br, N and Na) was detected by XPS (Fig. 1c), which excludes the possibility of existence of potential counterions such as Cl^-, Br^-, $[N(C_8H_{17})_4]^+$ and Na^+; thus, the as-prepared nanoparticle is neutral. Quantitative measurement reveals that the Au/S atomic ratio is 38.0:24.3 (Supplementary Figs 3 and 4), in good agreement with the expected ratio (38.0:24.0) for the composition of $Au_{38}(PET)_{24}$. Thus, the formula is identical to that of the nanoparticle previously reported in ref. 31; however, the absorption spectrum of our nanoparticle distinctly differs from that of the previous nanoparticle. The ultraviolet–visible–near-infrared spectrum of the novel $Au_{38}(PET)_{24}$ (abbreviated as Au_{38T}) shows six absorption peaks at 505 nm (ε: 3.86 gcml^{-1}), 540 nm (ε: 3.22 gcml^{-1}), 610 nm (ε: 1.46 gcml^{-1}), 700 nm (ε: 0.69 gcml^{-1}), 880 nm and 1,090 nm (Fig. 1d and Supplementary Fig. 2). The previous $Au_{38}(PET)_{24}$ (abbreviated as Au_{38Q}) shows six absorption peaks centred at 480 nm (ε: 4.62 gcml^{-1}), 520 nm (ε: 3.72 gcml^{-1}), 570 nm (ε: 2.86 gcml^{-1}), 627 nm (ε: 2.59 gcml^{-1}), 740 nm (ε: 0.58 gcml^{-1}) and 1,035 nm (Fig. 1d and Supplementary Fig.1). TLC also indicates that they are not the same nanoparticle (Fig. 1d, inset). Indeed, they are a pair of structural isomers (vide infra).

Atomic structure. The structure of the previous Au_{38Q} was determined by SCXC and it has a core-shell structure consisting of a face-fused bi-icosahedral Au_{23} core, which is capped by a second shell composed of the remaining 15 gold atoms (Fig. 2f). To confirm that our nanoparticle (Au_{38T}) is an isomer of Au_{38Q}, we grew high-quality single crystals and successfully elucidated the structure via SCXC. Briefly, the new structure of Au_{38T} is composed of one Au_{23} core and one mixed capping layer of thiolate ligands and gold–thiolate complex units. The Au_{23} core consists of one icosahedral Au_{13} and one Au_{10} unit, and the mixed surface layer contains two $Au_3(SR)_4$ staple units, three $Au_2(SR)_3$ staple units, three $Au_1(SR)_2$ staple units and one bridging thiolate SR ligand. The anatomy of the Au_{38T} structure starts with the central Au_{23} core (Fig. 2b), which can be viewed as one Au_{12} cap and one Au_{13} icosahedron (Fig. 2a) fused together via sharing two gold atoms (Fig. 2b, dark green gold atoms), which is in distinct contrast with the case of Au_{38Q}; for the latter, the two Au_{13} icosahedra are fused together via sharing a face (three gold atoms) to form a bi-icosahedral Au_{23} core. The Au_{12} cap is composed of three tetrahedra and the Au–Au bond lengths in each tetrahedron range from 2.71 to 2.88 Å. In the Au_{13} icosahedron, the Au–Au bond lengths between the central atom and the shell Au atoms (except for the two shared gold atoms) vary from 2.71 to 2.82 Å. The bond lengths between the two shared gold atoms and the central atom of Au_{13} icosahedron are 2.77 and 2.78 Å, respectively. The different Au_{23} core in Au_{38T} (in contrast to the biicosahedral Au_{23} core of Au_{38Q}) leads to various surface-binding structures. The Au_{23} core in our case was capped by two $Au_3(SR)_4$ units and two $Au(SR)_2$ units, and the average Au–S bond lengths/Au–S–Au bond angles were 2.33 Å/96.47° and 2.32 Å/94.43° in the $Au_3(SR)_4$ and $Au(SR)_2$ staple units, respectively (Fig. 2c). Interestingly, in addition to the two $Au_3(SR)_4$ units and two $Au(SR)_2$ units, one bridging thiolate (SR) is also found to link the Au_{13} icosahedron and the Au_{12} cap (Fig. 2c, the sulfur atom is marked in red), the two Au–S bond lengths are 2.33 and 2.30 Å, respectively, and the Au–S–Au bond angle is 92.66°. It is noteworthy that in Au_{38Q}, the Au_{23} core was protected by six $Au_2(SR)_3$ and three $Au(SR)_2$ staple units; no comparable $Au_3(SR)_4$ staple units and bridging thiolate (SR) was observed. The Au_{13} icosahedron in Au_{38T} is exclusively capped by two $Au_2(SR)_3$ staple units (the average Au–S bond lengths in the $Au_2(SR)_3$ staple units are 2.35 and 2.34 Å, respectively, and the

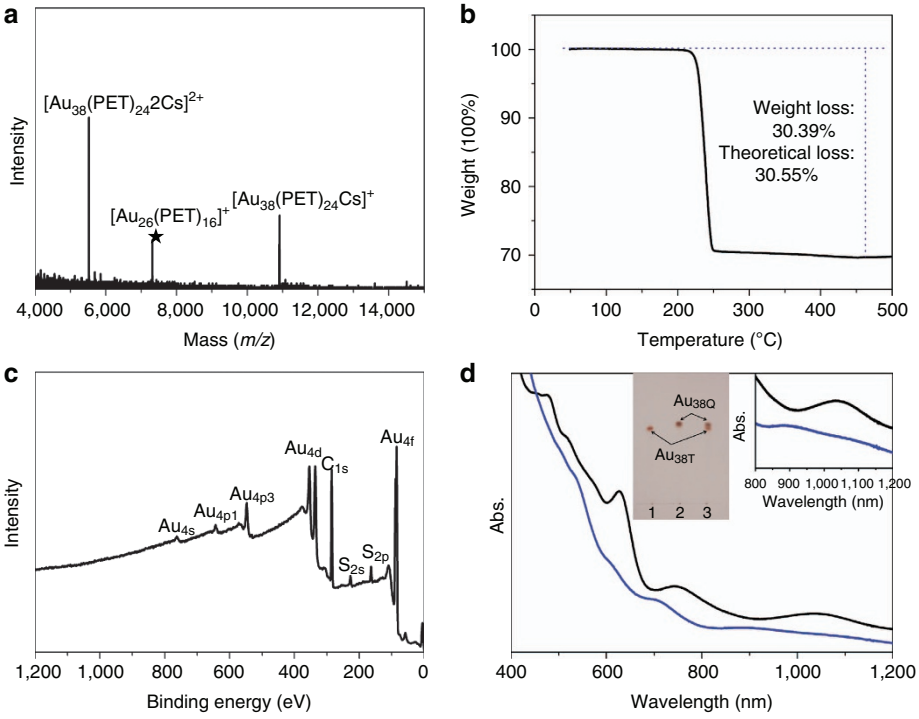

Figure 1 | Characteriztion of Au_{38T}. (**a**) ESI mass spectrum of the Au_{38T}. (**b**) TGA of Au_{38T}. (**c**) XPS spectrum of Au_{38T}. (**d**) Ultraviolet–visible–near-infrared absorption spectra of Au_{38T} (blue) and Au_{38Q} (black) in toluene (measurement temperature: 0 °C). Insets are the photo of thin-layer chromatography, and enlarged absorption spectra in the range from 800 to 1,200 nm of Au_{38T} and Au_{38Q}.

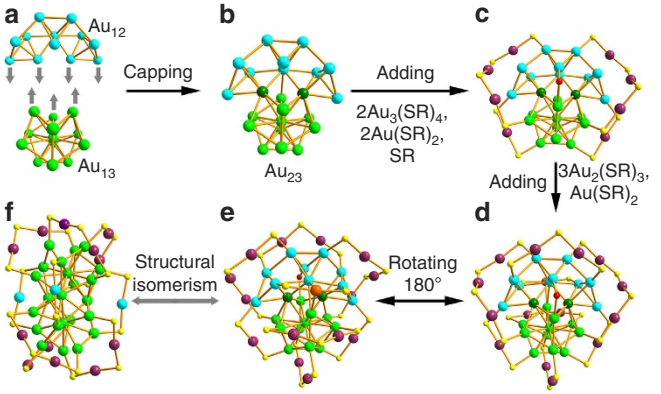

Figure 2 | Structures of Au_{38T} and Au_{38Q}. (**a**) Anatomy of the Au_{23} core, which consists of a Au_{12} cap unit and Au_{13} icosahedral unit. (**b**) Au_{23} core, which is constructed by one Au_{12} unit and one Au_{13} unit sharing two gold atoms. (**c**) Two $Au_3(SR)_4$, two $Au(SR)_2$ and one SR linking the Au_{12} cap and Au_{13} icosahedron. (**d**) Three $Au_2(SR)_3$ and one $Au(SR)_2$ protecting the Au_{23} core. (**e**) Back view of Au_{38T}. (**f**) The Au_{38Q} structure.

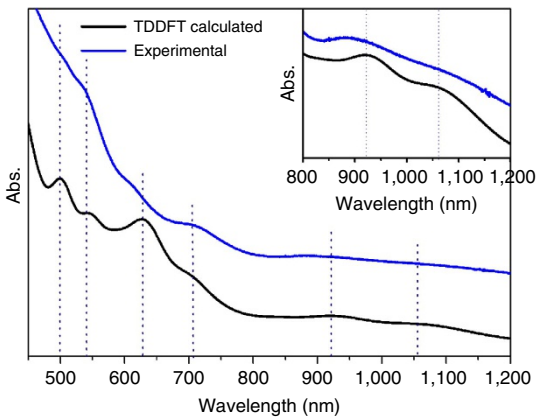

Figure 3 | Comparison of ultraviolet–visible–near-infrared absorption spectra of Au_{38T}. Blue: experimental; black: calculated by time-dependent density function (TDDFT) method. Inset is the enlarged spectra in the range from 800 to 1,200 nm.

average Au–S–Au bond angles in the $Au_2(SR)_3$ staple units are 92.20° and 90.33°, respectively) and the Au_{12} cap is capped by one $Au_2(SR)_3$ staple unit (the average Au–S bond length is 2.33 Å and the average Au–S–Au bond angle is 97.03°). In addition, the Au_{12} cap is also capped by one $Au(SR)_2$ staple unit, and the average Au–S bond length/Au–S–Au bond angle are 2.33 Å and 99.91° (Fig. 2d). The structure resolved by X-ray diffraction was further analysed by computations: the simulated ultraviolet–visible–near-infrared spectrum is close to the experimental one (Fig. 3).

As discussed above, the structure of Au_{38T} is remarkably different from that of Au_{38Q} and the main differences between the two structures lie in the type of Au_{23} core and the surface capping mode of the Au_{23} core. Au_{38T} and Au_{38Q} have an identical composition but completely different structures; thus, they are literally a pair of structural isomers. Notably, the structure of Au_{38T} reported in this work is novel and also differs from those theoretical structures predicted by Hakkinen *et al.*[37], Tsukuda and colleagues[38], Jiang *et al.*[39] and Zeng and colleagues[40], among others.

Transformation. Au_{38T} exhibits relatively high stability at low temperatures, as no obvious spectral changes was detected when a solution of Au_{38T} was stored at −10 °C for as long as 1 month in toluene (Fig. 4a). However, the absorption spectrum of Au_{38T} gradually changed to that of Au_{38Q} at 50 °C in toluene (Fig. 4b), which indicates that Au_{38T} can transform to Au_{38Q} at elevated

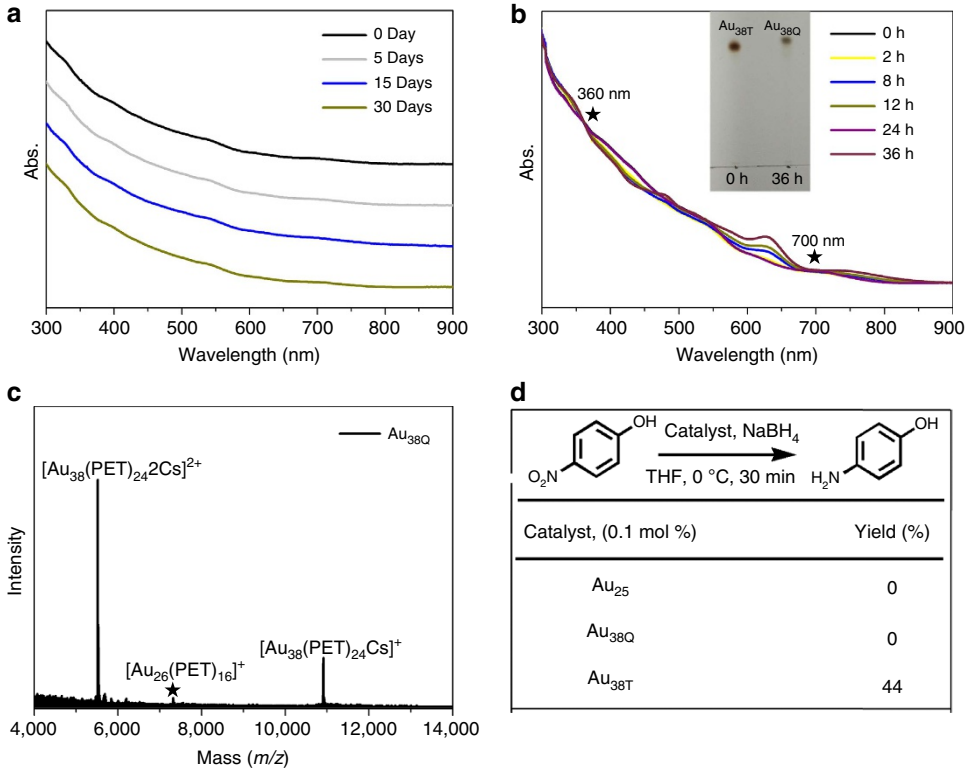

Figure 4 | Difference in stability and catalysis between Au_{38T} and Au_{38Q}. (**a**) Time-dependent ultraviolet–visible–near-infrared absorption spectra of Au_{38T} at −10 °C in toluene. (**b**) Ultraviolet–visible–near-infrared absorption spectral transformation at 50 °C in toluene (the isosbestic points are at 360 and 700 nm). Inset: thin-layer chromatography of Au_{38T} before and after the transformation. (**c**) ESI mass spectrum of the transformed product. (**d**) Catalytic activities of Au_{25}, Au_{38T} and Au_{38Q}.

temperatures. TLC and ESI–MS further support this transformation (Fig. 4b (inset) and Fig. 4c). However, the reverse transformation (that is, from Au_{38Q} to Au_{38T}) was not successful under various investigated conditions. These results indicate that Au_{38T} is less stable than Au_{38Q}, and that Au_{38T} can only be irreversibly transformed to Au_{38Q}. The reason for why the relatively unstable Au_{38T} is formed rather than the stable Au_{38Q} during the synthesis is probably because the former is kinetically favourable in our reaction conditions, similar to some previous reports[41,42].

Catalysis. Au_{38T} exhibits remarkably higher catalytic activity than Au_{38Q} at low temperature (for example, 0 °C) in reduction reactions. For example, 4-nitrophenol can be reduced to 4-aminophenol in 44% yield with 0.1 mol% Au_{38T} catalyst in half an hour, whereas no reduction occurred when $Au_{25}(PET)_{18}^{-}$ TOA^{+} (Au_{25} for short, TOA^{+}: tetra-*n*-octylammonium) or Au_{38Q} was used as the catalyst (Fig. 4d and Supplementary Fig. 5) under the same reaction conditions. It is noteworthy that in other cases, Au_{25} was reported to exhibit good catalytic reduction activity[43,44]. The high catalytic activity of Au_{38T} may be due to its surface being not as densely protected as the surfaces of Au_{25} and Au_{38Q}; further investigation is underway. A previous work[44] implied that the catalytic properties of gold nanoclusters are not only size dependent but also structure sensitive. However, the structure dependence of catalytic properties was unclear at that time, because the ligands were different in $Au_{44}(PET)_{32}$ and $Au_{44}(TBBT)_{28}$ (TBBT: 4-tert-butylbenzenethiolate), and the ligand effect should be considered. Herein, it is unambiguously demonstrated that the structure effect indeed exists, because Au_{38T} and Au_{38Q} exhibit remarkably different catalytic performance. Au_{38T} is relatively robust and can retain its ultraviolet–visible–near-infrared spectrum even after 18 catalytic cycles (Supplementary Fig. 6). It is noteworthy that the gradual decrease in the yield is primarily due to the unavoidable mass loss of the catalyst during the isolation by column chromatography. However, after 21 cycles, the catalyst transformed to more stable Au_{38Q} demonstrated by the ultraviolet–visible–near-infrared spectra and accordingly the loss of catalytic activity (see Supplementary Table 1). The high catalytic activity at low temperatures indicates the potential application of Au_{38T} in some catalytic processes.

Discussion

In summary, we have discovered a pair of structural isomers Au_{38T} and Au_{38Q}, which were identified using ESI–MS, TGA, XPS and SCXC. Although both species have the same composition (that is, $Au_{38}(PET)_{24}$), they have distinctly different structures, which results in differences in their optical and catalytic properties, as well as structural stability. The less stable Au_{38T} can be irreversibly transformed to the more stable Au_{38Q} at high temperatures. The structure of Au_{38T} is very interesting: it is composed of a Au_{23} core (fused by one Au_{13} icosahedron and one Au_{12} cap by sharing two atoms) and a mixed layer of thiolate ligands and gold–thiolate complex units for surface protection. This structure is unique (that is, not found in other reported gold nanoclusters). In particular, the diversity of staple units and the bridging thiolate found in Au_{38T} provide a new direction for structural studies of metal nanoclusters. The significance and novelty of this work are as follows. (i) A novel synthesis method is developed, with which a novel gold nanoparticle is readily synthesized, and the composition of the as-prepared nanoparticle is precisely determined using ESI–MS in conjunction with XPS and TGA. (ii) The structure of Au_{38T} is resolved using SCXC and the unique structural features provide important implications for

nanocluster structural studies. (iii) Significantly, structural isomerism is observed in nanoparticles for the first time. (iv) The distinctly different properties (in particular the catalytic properties) of the two structural isomers indicate a structure–property correlation and this will have important implications for future catalytic studies. It is expected that our work may motivate more studies on structural isomerism and structure–property correlations in nanoscale or even larger scale materials.

Methods

Reagents. All chemicals and reagents are commercially available and were used as received. Tetraoctylammonium bromide (TOAB, 98.0%) and 4-nitrophenol (99.0%) were obtained from Aladdin; 2-phenylethanethiol (PhC_2H_4SH, 99.0%) was purchased from Sigma-Aldrich; Au_{38Q} and $Au_{25}(PET)_{18}^{-}TOA^{+}$ were synthesized following reported methods[31,34].

Synthesis. Au_{38T} was synthesized using a modified one-pot method and separated using PTLC. Briefly, $HAuCl_4 \bullet 4H_2O$ (0.20 g, 0.48 mmol) was mixed with 1.03 equivalents of TOAB (0.27 g, 0.49 mmol) in CH_2Cl_2 (40 ml). Then, 9 equivalents of phenylethanethiol (0.61 ml, 4.50 mmol) were added to this solution and the solution was stirred for ~2 h until it became colourless. To this solution, 5.3 equivalents of $NaBH_4$ (0.11 g, 2.80 mmol) in cold water (5 ml) was added in one shot under vigorous stirring and the reaction was allowed to proceed under constant stirring for 6 h. CH_2Cl_2 was removed via rotary evaporation at 20 °C to isolate the crude product. For purification, the crude product was extracted with a small amount of tetrahydrofuran (THF) and washed with ice water three times and with CH_3OH two times; during this procedure, traces of inorganic salt, excess TOAB and phenylethanethiol were thoroughly removed. Next, the as-obtained crude products were separated using PTLC (dichloromethane: petroleum ether = 3:4) and finally the target product was isolated from the reddish brown band of PTLC after extraction with CH_2Cl_2, with a yield of 5%.

Characterization. The ultraviolet–visible–near-infrared absorption spectrum was measured on a UV-3600 spectrophotometer (Shimadzu, Japan) at room temperature. TGA analysis was conducted under a N_2 atmosphere (~3 mg sample used, flow rate ~50 ml min^{-1}) on a TG/DTA 6300 analyzer (Seiko Instruments, Inc.) and the heating rate was 10 °C min^{-1}. XPS measurements were performed on an ESCALAB 250Xi XPS spectrometer (Thermo Scientific, USA), using a monochromated Al Kα source and equipped with an Ar^{+} ion sputtering gun. All binding energies were calibrated using the C (1 s) carbon peak (284.8 eV). ESI–MS data were acquired on a Waters Q-TOF mass spectrometer equipped with a Z-spray source. The sample was dissolved in toluene (~1 mg ml^{-1}) and diluted 1:1 in dry ethanol (5 mM CsOAc). The sample was directly infused at 5 µl min^{-1}. The source temperature was fixed at 70 °C. The spray voltage was set at 2.20 kV and the cone voltage was set at 60 V.

Single-crystal growth and analysis. Black crystals were formed from a CH_2Cl_2/hexane solution of the nanoclusters at 4 °C after 5 days. The diffraction data for $Au_{38}(PET)_{24}$ were collected at 173 K on a Bruker APEX DUO X-ray diffractometer using Cu Kα radiation ($\lambda = 1.54184$ Å).

Theoretical methods. All calculations were performed using density functional theory with the pure functional Perdew-Burke-Ernzerhof[45,46] and the all electron basis set 6–31 g (*d*, *p*) for H, S, pseudopotential basis set LANL2DZ for Au, as implemented in the Gaussian 09 program package[47]. Time-dependent density functional calculations[48] were performed to reproduce the experimental ultraviolet–visible spectrum and –R group was replaced by –H to minimize computational work[31]. The Gaussian half-width at half-height of 0.15 eV in the Multiwfn software[49] was used to simulate the ultraviolet–visible spectrum.

General procedure for the catalyses. 4-Nitrophenol (69.50 mg, 0.500 mmol), Au_{38Q}, Au_{25} or Au_{38T} (0.100 mol%, not adsorbed on a support or calcined) and THF (5 ml) were mixed in a reaction tube at 0 °C. The mixture was stirred at this temperature for 5 min. $NaBH_4$ (189.00 mg, 5.000 mmol) dissolved in 1.0 ml of H_2O was added slowly to the mixture. After stirring at 0 °C for 30 min, a large amount of water was added to quench the reaction. The mixture was extracted with dichloromethane twice (2 × 10 ml) and then the organic layers were collected and concentrated. The reduction product (4-aminophenol) was purified by column chromatography on silica gel, with ethyl acetate and petroleum ether (ethyl acetate/petroleum ether = 1/1) as the eluant.

General procedure for the recovery of Au_{38T}. When the reduction was completed, the reaction mixture was quenched with water. Au_{38T} and other organic compounds were extracted with dichloromethane. The extract was collected and concentrated. After the other organic compounds were isolated by column chromatography with ethyl acetate and petroleum ether, Au_{38T} was recovered using dichloromethane as the eluant. The dichloromethane was evaporated under reduced pressure and then Au_{38T} was re-used in the next cycle without further treatment.

References

1. Billinge, S. J. & Levin, I. The problem with determining atomic structure at the nanoscale. *Science* **316,** 561–565 (2007).
2. Akola, J., Walter, M., Whetten, R. L., Hakkinen, H. & Gronbeck, H. On the structure of thiolate-protected Au_{25}. *J. Am. Chem. Soc.* **130,** 3756–3757 (2008).
3. Weissker, H. C., Lopez-Acevedo, O., Whetten, R. L. & López-Lozano, X. optical spectra of the special Au_{144} gold-cluster compounds: sensitivity to structure and symmetry. *J. Phys. Chem. C.* **119,** 11250–11259 (2015).
4. Gruene, P. *et al.* Structures of neutral Au_7, Au_{19}, and Au_{20} clusters in the gas phase. *Science* **321,** 674–676 (2008).
5. Olson, R. M. & Gordon, M. S. Isomers of Au 8. *J. Chem. Phys.* **126,** 214310–214316 (2007).
6. Pyykko, P. Theoretical chemistry of gold. III. *Chem. Soc. Rev.* **37,** 1967–1997 (2008).
7. Huang, W., Pal, R., Wang, L. -M., Zeng, X. C. & Wang, L. -S. Isomer identification and resolution in small gold clusters. *J. Chem. Phys.* **132,** 054305–054305 (2010).
8. Schaefer, B. *et al.* Isomerism and structural fluxionality in the Au_{26} and Au_{26}^{-} nanoclusters. *ACS Nano* **8,** 7413–7422 (2014).
9. Brust, M., Walker, M., Bethell, D., Schiffrin, D. J. & Whyman, R. Synthesis of thiol-derivatized gold nanoparticles in a 2-phase liquid-liquid system. *Chem. Commun.* **7,** 801–802 (1994).
10. Qian, H. & Jin, R. Controlling nanoparticles with atomic precision: the case of $Au_{144}(SCH_2CH_2Ph)_{60}$. *Nano Lett.* **9,** 4083–4087 (2009).
11. Ackerson, C. J., Jadzinsky, P. D. & Kornberg, R. D. Thiolate ligands for synthesis of water-soluble gold clusters. *J. Am. Chem. Soc.* **127,** 6550–6551 (2005).
12. Fields-Zinna, C. A., Sardar, R., Beasley, C. A. & Murray, R. W. Electrospray ionization mass spectrometry of intrinsically cationized nanoparticles, $Au_{144/146}(SC_{11}H_{22}N(CH_2CH_3)_3^{+})_x(S(CH_2)_5CH_3)_y^{x+}$. *J. Am. Chem. Soc.* **131,** 16266–16271 (2009).
13. Sardar, R., Funston, A. M., Mulvaney, P. & Murray, R. W. Gold nanoparticles: past, present, and future. *Langmuir.* **25,** 13840–13851 (2009).
14. Lopez-Acevedo, O., Kacprzak, K. A., Akola, J. & Hakkinen, H. Quantum size effects in ambient CO oxidation catalysed by ligand-protected gold clusters. *Nat. Chem.* **2,** 329–334 (2010).
15. Hakkinen, H. The gold-sulfur interface at the nanoscale. *Nat. Chem.* **4,** 443–455 (2012).
16. Lu, Y. Z. & Chen, W. Sub-nanometre sized metal clusters: from synthetic challenges to the unique property discoveries. *Chem. Soc. Rev.* **41,** 3594–3623 (2012).
17. Qian, H. F., Zhu, Y. & Jin, R. C. Atomically precise gold nanocrystal molecules with surface plasmon resonance. *Proc. Natl Acad. Sci. USA* **109,** 696–700 (2012).
18. Yau, S. H., Varnavski, O. & Goodson, T. An ultrafast look at Au nanoclusters. *Acc. Chem. Res.* **46,** 1506–1516 (2013).
19. Weissker, H. C. *et al.* Information on quantum states pervades the visible spectrum of the ubiquitous $Au_{144}(SR)_{60}$ gold nanocluster. *Nat. Commun.* **5,** 3785 (2014).
20. Yu, Y. *et al.* Solvent controls the formation of $Au_{29}(SR)_{20}$ nanoclusters in the CO-reduction method. *Part. Part. Syst. Char.* **31,** 652–656 (2014).
21. Jadzinsky, P. D., Calero, G., Ackerson, C. J., Bushnell, D. A. & Kornberg, R. D. Structure of a thiol monolayer-protected gold nanoparticle at 1.1A resolution. *Science* **318,** 430–433 (2007).
22. Heaven, M. W., Dass, A., White, P. S., Holt, K. M. & Murray, R. W. Crystal structure of the gold nanoparticle $[N(C_8H_{17})_4][Au_{25}(SCH_2CH_2Ph)_{18}]$. *J. Am. Chem. Soc.* **130,** 3754–3755 (2008).
23. Zhu, M., Aikens, C. M., Hollander, F. J., Schatz, G. C. & Jin, R. Correlating the crystal structure of A thiol-protected Au_{25} cluster and optical properties. *J. Am. Chem. Soc.* **130,** 5883–5885 (2008).
24. Qian, H., Eckenhoff, W. T., Zhu, Y., Pintauer, T. & Jin, R. Total structure determination of thiolate-protected Au_{38} nanoparticles. *J. Am. Chem. Soc.* **132,** 8280–8281 (2010).
25. Zeng, C. *et al.* Total structure and electronic properties of the gold nanocrystal $Au_{36}(SR)_{24}$. *Angew. Chem. Int. Ed.* **51,** 13114–13118 (2012).
26. Malola, S. *et al.* $Au_{40}(SR)_{24}$ cluster as a chiral dimer of 8-electron superatoms: structure and optical properties. *J. Am. Chem. Soc.* **134,** 19560–19563 (2012).
27. Jiang, D. E., Overbury, S. H. & Dai, S. Structure of $Au_{15}(SR)_{13}$ and its implication for the origin of the nucleus in thiolated gold nanoclusters. *J. Am. Chem. Soc.* **135,** 8786–8789 (2013).
28. Yang, H., Wang, Y., Edwards, A. J., Yan, J. & Zheng, N. High-yield synthesis and crystal structure of a green Au_{30} cluster co-capped by thiolate and sulfide. *Chem. Commun.* **50,** 14325–14327 (2014).

29. Das, A. *et al.* Crystal structure and electronic properties of a thiolate-protected Au_{24} nanocluster. *Nanoscale* **6,** 6458–6462 (2014).
30. Song, Y. *et al.* Crystal structure of selenolate-protected $Au_{24}(SeR)_{20}$ nanocluster. *J. Am. Chem. Soc.* **136,** 2963–2965 (2014).
31. Qian, H., Zhu, Y. & Jin, R. Size-focusing synthesis, optical and electrochemical properties of monodisperse $Au_{38}(SC_2H_4Ph)_{24}$ nanoclusters. *ACS Nano.* **3,** 3795–3803 (2009).
32. Wang, Z. W., Toikkanen, O., Quinn, B. M. & Palmer, R. E. Real-space observation of prolate monolayer-protected Au_{38} clusters using aberration-corrected scanning transmission electron microscopy. *Small* **7,** 1542–1545 (2011).
33. Dolamic, I., Knoppe, S., Dass, A. & Burgi, T. First enantioseparation and circular dichroism spectra of Au_{38} clusters protected by achiral ligands. *Nat. Commun.* **3,** 798 (2012).
34. Wu, Z., Suhan, J. & Jin, R. One-pot synthesis of atomically monodisperse, thiol-functionalized Au_{25} nanoclusters. *J. Mater. Chem.* **19,** 622–626 (2009).
35. Ghosh, A. *et al.* Simple and efficient separation of atomically precise noble metal clusters. *Anal. Chem.* **86,** 12185–12190 (2014).
36. Yao, C. *et al.* Adding two active silver atoms on Au nanoparticle. *Nano Lett.* **15,** 1281–1287 (2015).
37. Hakkinen, H., Walter, M. & Gronbeck, H. Divide and protect: apping gold nanoclusters with molecular gold-thiolate rings. *J. Phys. Chem. B.* **110,** 9927–9931 (2006).
38. Lopez-Acevedo, O., Tsunoyama, H., Tsukuda, T., Hakkinen, H. & Aikens, C. M. Chirality and electronic structure of the thiolate-protected Au_{38} nanocluster. *J. Am. Chem. Soc.* **132,** 8210–8218 (2010).
39. Jiang, D. E., Luo, W., Tiago, M. L. & Dai, S. In search of a structural model for a thiolate-protected Au_{38} cluster. *J. Phys. Chem. C.* **112,** 13905–13910 (2008).
40. Pei, Y., Gao, Y. & Zeng, X. C. Structural prediction of thiolate-protected Au_{38}: a face-fused bi-icosahedral Au core. *J. Am. Chem. Soc.* **130,** 7830–7832 (2008).
41. Wu, Z., MacDonald, M. A., Chen, J., Zhang, P. & Jin, R. Kinetic control and thermodynamic selection in the synthesis of atomically precise gold nanoclusters. *J. Am. Chem. Soc.* **133,** 9670–9673 (2011).
42. Yuan, X. *et al.* Balancing the rate of cluster growth and etching for gram-scale synthesis of thiolate-protected Au_{25} nanoclusters with atomic precision. *Angew. Chem. Int. Ed.* **53,** 4623–4627 (2014).
43. Shivhare, A., Ambrose, S. J., Zhang, H., Purves, R. W. & Scott, R. W. Stable and recyclable Au_{25} clusters for the reduction of 4-nitrophenol. *Chem. Commun.* **49,** 276–278 (2013).
44. Li, M. -B., Tian, S. -K., Wu, Z. & Jin, R. Cu^{2+} induced formation of $Au_{44}(SC_2H_4Ph)_{32}$ and its high catalytic activity for the reduction of 4-nitrophenol at low temperature. *Chem. Commun.* **51,** 4433–4436 (2015).
45. Perdew, J. P., Burke, K. & Ernzerhof, M. Generalized gradient approximation made simple. *Phys. Rev. Lett.* **77,** 3865–3868 (1996).
46. Perdew, J. P., Burke, K. & Ernzerhof, M. Generalized gradient approximation made simple (vol 77, pg 3865, 1996). *Phys. Rev. Lett.* **78,** 1396–1396 (1997).
47. Frisch, M. J. *et al. Gaussian 09, Revision B.01* (Gaussian, Inc., 2010).
48. Perdew, J. P. *et al.* Prescription for the design and selection of density functional approximations: more constraint satisfaction with fewer fits. *J. Chem. Phys.* **123,** 062001–062009 (2005).
49. Lu, T. & Chen, F. Multiwfn: a multifunctional wavefunction analyzer. *J. Comput. Chem.* **33,** 580–592 (2012).

Acknowledgements

Z.W. thank the National Basic Research Program of China (grant number 2013CB934302), the Natural Science Foundation of China (numbers 21222301 and 21171170), the Ministry of Human Resources and Social Security of China, the Innovative Program of Development Foundation of Hefei Center for Physical Science and Technology (2014FXCX002), the CAS/SAFEA International Partnership Program for Creative Research Teams and the Hundred Talents Program of the Chinese Academy of Sciences for financial support. R.J. acknowledges financial support from the U.S. Department of Energy-Office of Basic Energy Sciences, Grant DE-FG02-12ER16354, and the Natural Science Foundation of China (Overseas, Hong Kong and Macao Scholars Collaborated Researching Fund, number 21528303). We greatly appreciate Professor Linhong Weng and Professor Yuejian Lin for the assistance in the single-crystal X-ray diffraction analysis. The calculations in this paper have been done on the supercomputing system in the Supercomputing Center of University of Science and Technology of China.

Author contributions

S.T. conceived and carried out the experiments. Y.L. resolved the structure. M.L. carried out the catalytic experiments. J. Yuan and J. Yang conducted computing. Z.W. and R.J. designed the study, supervised the project and analysed the data. All authors contributed to the preparation of the manuscript.

Additional information

Accession codes: The X-ray crystallographic coordinates for structures reported in this study (see Supplementary Table 2 and Supplementary Data 1) have been deposited at the Cambridge Crystallographic Data Centre (CCDC), under deposition number CCDC 1423153. These data can be obtained free of charge from The Cambridge Crystallographic Data Centre via www.ccdc.cam.ac.uk/data_request/cif.

Supplementary Information accompanies this paper at http://www.nature.com/naturecommunications

Competing financial interests: The authors declare no competing financial interests.

Reprints and permission information is available online at http://npg.nature.com/reprintsandpermissions/

How to cite this article: Tian, S. *et al.* Structural isomerism in gold nanoparticles revealed by X-ray crystallography. *Nat. Commun.* 6:8667 doi: 10.1038/ncomms9667 (2015).

nature COMMUNICATIONS

DOI: 10.1038/ncomms10012 OPEN

Erratum: Structural isomerism in gold nanoparticles revealed by X-ray crystallography

Shubo Tian, Yi-Zhi Li, Man-Bo Li, Jinyun Yuan, Jinlong Yang, Zhikun Wu & Rongchao Jin

Nature Communications 6:8667 doi: 10.1038/ncomms9667 (2015); Published 20 Oct 2015; Updated 17 Nov 2015

The original version of this Article contained an error in the spelling of isomerism in the title of the paper. This has now been corrected in both the PDF and HTML versions of the Article.